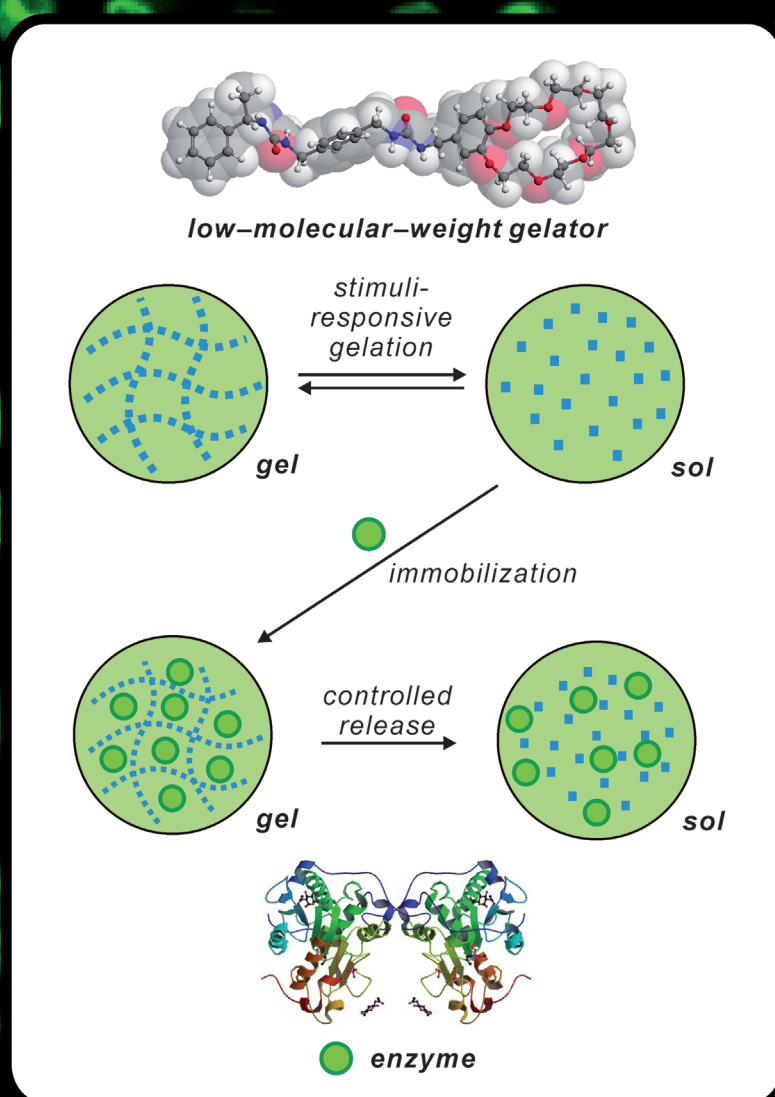


Fibrous Networks with Incorporated Macrocycles: A Chiral Stimuli-Responsive Supramolecular Supergelator and Its Application to Biocatalysis in Organic Media

Zhenhui Qi,^[a] Changzhu Wu,^[a] Paula Malo de Molina,^[b] Han Sun,^[c] Andrea Schulz,^[a] Christian Griesinger,^[c] Michael Gradzielski,^[b] Rainer Haag,^[a] Marion B. Ansorge-Schumacher,^[b, d] and Christoph A. Schalley*^[a]

Dedicated to Professor Dr. Jörn Manz on the occasion of his 65th birthday

Supramolecular Gels



Abstract: A new and versatile, crown ether appended, chiral supergelator has been designed and synthesized based on the bis-urea motif. The introduction of a stereogenic center improved its gelation ability significantly relative to its achiral analogue. This low-molecular-weight gelator forms supramolecular gels in a variety of organic solvents. It is sensitive to multiple chemical stimuli and the sol–gel phase transitions can

be reversibly triggered by host–guest interactions. The gel can be used to trap enzymes and release them on demand by chemical stimuli. It stabilizes the microparticles in Pickering emulsions so that enzyme-catalyzed organic

reactions can take place in the polar phase inside the microparticles, the organic reactants diffusing through the biphasic interface from the surrounding organic phase. Because of the higher interface area between the organic and polar phases, enzyme activity is enhanced in comparison with simple biphasic systems.

Keywords: biocatalysis • crown compounds • gels • host–guest systems • self-assembly

Introduction

Natural fibrous networks such as microtubuli or actin filaments are self-assembled noncovalent architectures that are essential for cytoskeleton construction and give cells their shape.^[1] Highly dynamic in assembly and disassembly, the fibers are equipped with sites for the recognition of, for example, the kinesin linear motors that, driven by adenosine triphosphate (ATP) hydrolysis, actively transport carriage along the microtubuli across the cell.^[2] Beyond their architectural role expressed in terms of cell shape, the fibrous network is thus also an integral part of the metabolism and behavior of the cell. Such function not only requires a high degree of hierarchical order, but also selective responsiveness to chemical signals in the microenvironment that controls the metabolism's complex spatio-temporal pattern development.

Synthetic fibrous networks in supramolecular gels^[3] certainly do not yet match the complexity and functional precision of their natural counterparts but can nevertheless be functional. On the one hand, their noncovalent nature makes them responsive^[4] to chemical stimuli that compete with the binding interactions between the individual gelator molecules^[5] and thus control the assembly or disassembly of gel fibers. More challenging, on the other hand, is to implement gelation control through interactions of the stimulus

with a molecular recognition unit attached to the fibers, which, however, is not directly involved in gel formation.^[6] Chemically triggered gel–sol transitions form the basis of functional materials^[7] with potential for drug delivery and cosmetics.^[8] A load trapped inside the cavities of a gel can be liberated on demand when a suitable chemical signal induces the gel–sol transition. Making two stimuli interdependent like the inputs of a logic gate can help define much more precisely under which conditions the gel–sol transition occurs.^[9] Function can also be based on the mechanical properties of the gel, for example, by using the gel as a matrix for immobilizing biocatalysts.^[10] As most enzymes operate best in water or polar solvents, their use in organic reactions is often limited unless the phase incompatibility is appropriately dealt with. This can be achieved either in emulsions that are stabilized by amphiphilic surfactants or in Pickering emulsions^[11,12] in which the enzyme-containing polar-phase droplets are stabilized by surrounding SiO₂ nanoparticles. Gelling of the polar phase inside these nanoparticle-surrounded droplets stabilizes them with the synthetic advantage that the droplets containing the enzyme can easily be reused by separating them from the reaction mixture by centrifugation.

Results and Discussion

Gelator synthesis and gel formation: The two enantiomers of the chiral low-molecular-weight gelator, (*R*)-**1** and (*S*)-**1** (Scheme 1), are bis-urea gelators^[13] equipped with a benzo-21-crown-7 ether.^[14] The crown ether represents a molecular recognition unit that makes the gelator susceptible to a variety of different chemical stimuli, presumably without being directly involved in gel formation. The cavity size of the crown is not only suitable for K⁺ binding, but also allows dialkylammonium ions to form pseudorotaxanes by threading through the crown ether.^[15] As a third chemical stimulus, competitive anions such as chloride can interfere with the urea–urea hydrogen bonding between adjacent gelator molecules.^[16]

The gelator enantiomers (*R*)-**1** and (*S*)-**1** were synthesized as summarized in Scheme 1. Mono-Boc-protected 1,4-bis-

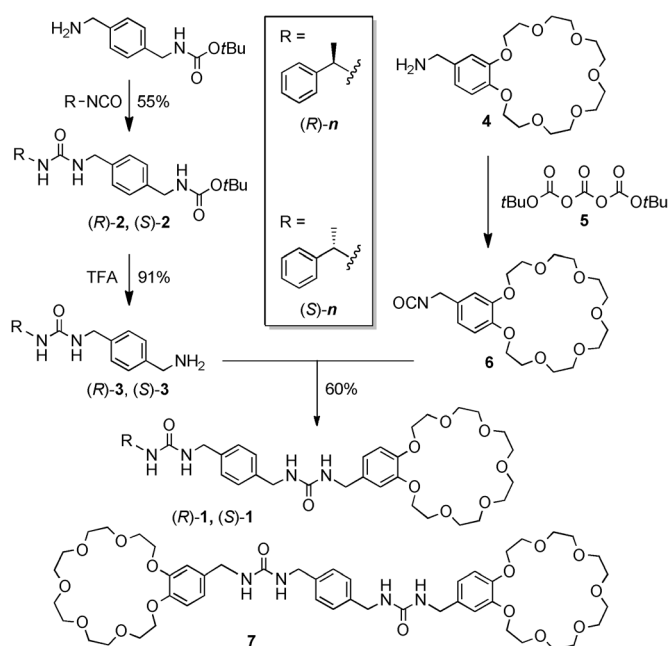
[a] Z. Qi, Dr. C. Wu, A. Schulz, Prof. R. Haag, Prof. C. A. Schalley
Institut für Chemie und Biochemie, Freie Universität Berlin
Takustr. 3, 14195 Berlin (Germany)
Fax: (+49) 30-838-55817
E-mail: christoph@schalley-lab.de

[b] Dr. P. Malo de Molina, Prof. M. Gradzielski,
Prof. M. B. Ansorge-Schumacher
Institut für Chemie, Technische Universität Berlin
Straße des 17. Juni 124, 10624 Berlin (Germany)

[c] H. Sun, Prof. C. Griesinger
Max-Planck-Institut für Biophysikalische Chemie
Am Fassberg 11, 37073 Göttingen (Germany)

[d] Prof. M. B. Ansorge-Schumacher
Current address: Institut für Mikrobiologie
Technische Universität Dresden, 01062 Dresden (Germany)

Supporting information for this article is available on the WWW
under <http://dx.doi.org/10.1002/chem.201300193>.



Scheme 1. Synthesis of chiral gelators (*R*)-**1** and (*S*)-**1**. Achiral bis-crown gelator **7** was prepared and characterized similarly as reported earlier.^[9b] It serves as a comparison here.

(aminomethyl)benzene was first converted into the chiral urea derivatives (*R*)-**2** and (*S*)-**2**, which were subsequently deprotected to yield (*R*)-**3** and (*S*)-**3**. To complete the gelator synthesis and incorporate the second urea moiety, the crown ether was attached to the free amino group as the isocyanate **6**, which was synthesized from the corresponding amine **4**^[9b] in situ. Although the synthesis of the gelator contains two steps that give only mediocre yields, it is quite efficient because the purification of all the intermediates and the final product can be achieved simply by precipitation, filtration, and washing. The elemental analysis of the final gelator molecules confirmed that a high purity was achieved without additional purification such as chromatography or recrystallization. As the chiral center is not affected by any of the synthetic procedures, the enantiomeric excess remains unchanged with respect to that of the commercially available (*R*)- or (*S*)-(-)- α -methylbenzyl isocyanate used as the reactant (*ee* $\geq 99\%$).

Enantiopure gelators (*R*)-**1** or (*S*)-**1** form gels (Table 1) with quite low critical gel concentrations (CGC) in a variety of different solvents, among them linear-chain alcohols, chlorinated hydrocarbons (CH_2Cl_2 and CHCl_3), 1,4-dioxane, nitromethane, and, in particular, acetonitrile. In this last solvent, (*R*)-**1**/*(S)*-**1** can be regarded as supergelators as gelation occurs at concentrations below 0.1 wt.%. In contrast, the gelator is insoluble in nonpolar solvents such as linear or cyclic alkanes and in aromatic hydrocarbons. At the other end of the polarity scale are solvents with high hydrogen-bond acceptor strengths such as dimethyl sulfoxide (DMSO) or dimethylformamide (DMF), in which the gelator dissolves without gel formation. With these gelation properties,

Table 1. Results of the gelation experiments with compound (*R*)-**1**.^[a]

Solvent	State	CGC ^[b]
<i>n</i> -butanol	gel	0.75 wt. %, 6 mg mL ⁻¹
<i>n</i> -propanol	gel	0.88 wt. %, 7 mg mL ⁻¹
ethanol	gel	1.64 wt. %, 13 mg mL ⁻¹
methanol	gel	1.25 wt. %, 10 mg mL ⁻¹
dichloromethane	gel	0.63 wt. %, 5 mg mL ⁻¹
chloroform	gel	0.38 wt. %, 3 mg mL ⁻¹
1,4-dioxane	gel	0.63 wt. %, 5 mg mL ⁻¹
nitromethane	gel	0.38 wt. %, 3 mg mL ⁻¹
acetonitrile	gel	0.10 wt. %, 0.8 mg mL ⁻¹
DMSO, DMF	solution	
ethyl acetate, <i>n</i> -butyl acetate	partial gel ^[c]	
tetrahydrofuran, isobutyl alcohol	partial gel ^[c]	
toluene, xylene	partial gel ^[c]	
cyclohexane, <i>n</i> -heptane, dodecane	insoluble	
diethyl ether, acetone, water	insoluble	

[a] All spectra were recorded at a concentration of 14 mg mL⁻¹. [b] For the gels, the 20 °C critical gelation concentrations (CGC) are given. The CGC is defined as the concentration below which no gel forms. [c] The term partial gel refers to a very viscous fluid.

gelator (*R*)-**1**/*(S)*-**1** is more versatile in terms of solvent choice and has a higher gelation ability than previously reported achiral gelator **7** bearing two benzo-21-crown-7 groups.^[9b]

FTIR experiments on the gels revealed N–H stretch vibrations at around 3318 cm⁻¹ and amide bands at around 1616 and 1568 cm⁻¹, which are typical of hydrogen-bonded urea groups (Table 2). Urea–urea hydrogen-bonding is thus

Table 2. FTIR data for (*R*)-**1** in the gel and solid state.^[a]

Solvent	Amide absorption bands [cm ⁻¹]		
	NH stretch	Amide-I	Amide-II
<i>n</i> -butanol	n.d. ^[b]	1616.4	1568.1
<i>n</i> -propanol	n.d. ^[b]	1616.7	1565.2
ethanol	n.d. ^[b]	1616.4	1564.4
methanol	n.d. ^[b]	1616.0	1565.8
dichloromethane	3319.0	1615.7	1568.3
chloroform	3313.4	1615.4	1569.4
1,4-dioxane	3318.7	1616.7	1566.6
nitromethane	3317.7	n.d. ^[c]	n.d. ^[c]
acetonitrile	3325.5	1616.1	1568.6
solid state	3318.7	1615.4	1565.3

[a] All spectra were recorded at a concentration of 14 mg mL⁻¹ at room temperature. [b] Not detected because bands are superimposed by the broad O–H stretch vibration band of the solvent. [c] Not detected, because bands are superimposed by the symmetric and antisymmetric stretch vibration bands of the nitro group of the solvent.

an important factor for gel formation.^[17] As reported earlier,^[18] an antiparallel arrangement of the two urea groups is pivotal for gelation. We assume this to be also true for (*R*)-**1** and (*S*)-**1**. On a macroscopic level, the gels of (*R*)-**1** or (*S*)-**1** in acetonitrile display typical thermoreversibility and are characterized by somewhat concentration-dependent gel–sol transition temperatures T_{gs} that range from 327 K for a gelator concentration of 5.0 mM to 354 K for a concentration of 25.0 mM (see Figure S15 in the Supporting Information).

Gel morphology and its formation mechanism: Because electron microscopy is problematic with acetonitrile as solvent, atomic force microscopy (AFM) was used to characterize the gel morphology (Figure 1). The AFM images show the formation of entangled networks of quite uniform, micrometer-long, straight helical fibers in the gels of both enantiomers, (*R*)-1 and (*S*)-1. The fibers strongly overlap in the gel state so that dilute samples were spin-coated on to mica to generate separate fibers suitable for a more detailed analysis. Well-defined right-handed *P* helices originate from (*R*)-1, whereas (*S*)-1 affords predominantly left-handed *M* helices (as labeled in Figure 1). In some images, a few diastereomeric fibers with the opposite helicity were also observed. This indicates the kinetically controlled co-formation of a minor amount of oppositely twisted fibers that are prevented from converting into the predominant helicity once they are formed by high activation barriers (see Figures S27 and S29 in the Supporting Information). Such a phenomenon was similarly observed in the self-assembly of gels formed from chiral merocyanine dyes.^[19] It also rationalizes the nonperfect mirror symmetry of the CD and VCD spectra (see Figure S16 in the Supporting Information) of the two gelator enantiomers: Depending on the exact conditions during gel formation, different amounts of the second type of fiber may form. As the two fibers have a diastereomeric relation to each other, the CD spectra may differ depending on their ratio. Overall, the methyl group at the chiral center exerts quite strong, but not perfect, control over the helicity of the fibers. The predominant helicity observed is in agreement with the results of semiempirical AM1 MOZYME calculations performed on a hexadecameric aggregate (see Figure S13 in the Supporting Information).^[20] In the calculations, the benzo-21-crown-7 ether was replaced by phenyl. When the calculated helices turn as observed by experiment, the methyl groups point sideways and thus find sufficient space to avoid steric repulsion with the next neighboring gelator molecule. If one performs a calculation on the opposite helix, the methyl groups are directed towards the neighboring gelator molecule causing higher steric strain.

AFM section analyses revealed a fiber height of around 6–7 nm with a helical pitch of around 47 nm (Figure 1c,f and Figures S32 and S33 in the Supporting Information). More precise information regarding the fiber diameter was obtained from small-angle neutron scattering (SANS) measurements (Figure 1g), which showed the fibers to be very well described by homogeneous cylinders with a diameter of 7.6 ± 0.2 nm (simulated data for differing cross-section diameters are given in Figure 1g and shows the substantial discrepancies occurring for other assumed diameters). Only for $q < 0.08 \text{ nm}^{-1}$ is a significant deviation of the experimental scattering data from the theoretical curve observed, which means that for sizes above 80–100 nm, deviations from a simple cylindrical structure are present. This upturn at low q can be ascribed to the formation of a network structure, in agreement with the structure observed by AFM (Figure 1a,d). It can also be noted that overall the structure is only little affected by the concentration in the studied range

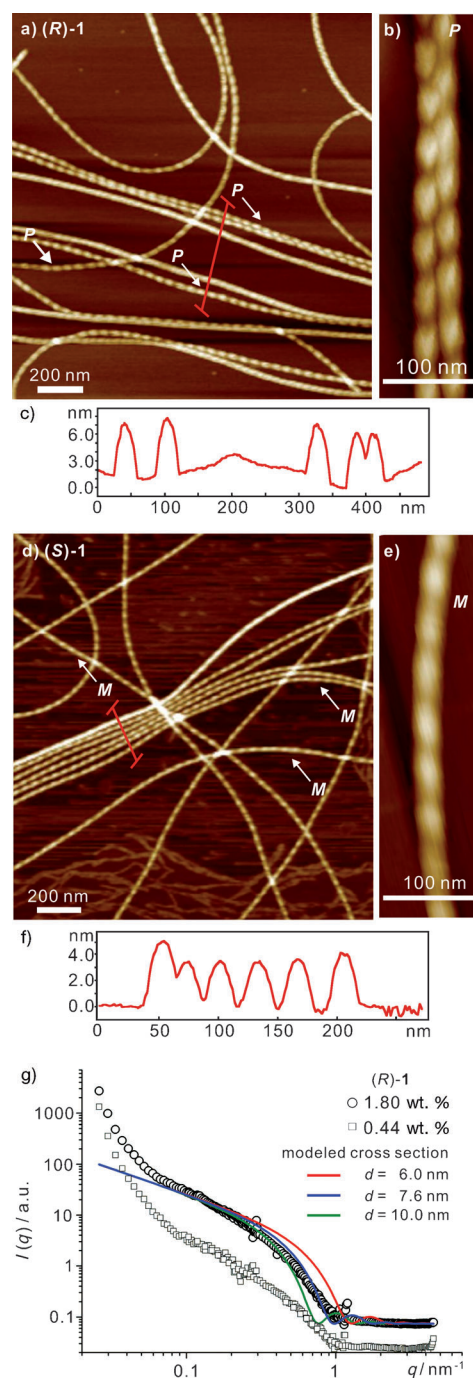
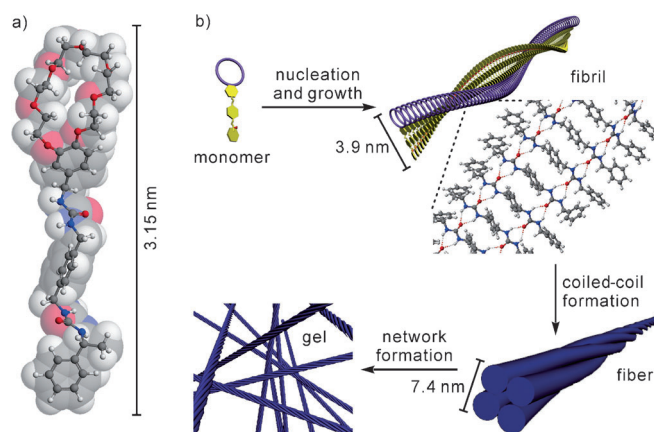


Figure 1. a,d) AFM height images ($1.6 \times 1.6 \mu\text{m}$) of samples prepared by spin-coating solutions of a) (*R*)-1 and d) (*S*)-1 obtained by the dilution of 0.127 wt. % chiral gels in acetonitrile to 0.05 and 0.025 wt. %, respectively. b,e) Enlarged AFM images of fibers formed from b) (*R*)-1 and e) (*S*)-1. c,f) Height profiles along the red lines indicated in images (a) and (d). g) SANS curves measured for gelator (*R*)-1 at concentrations of 1.80 wt. % (\circ) and 0.44 wt. % (\square) as a function of the scattering vector q in deuterated acetonitrile. The colored solid lines correspond to fits to infinitely long cylinders with different cross-sections. Cylinders with diameters of 7.4 nm give the best fit to the experimental data. The upturn of the intensity at low q indicates network formation.

of 0.44–1.80 wt. %. The somewhat smaller height determined by AFM may be rationalized by flattening of the fibers

during sample drying. The diameter of the fiber is consequently about twice that of the calculated monomer length of around 3.15 nm. Interestingly, in some AFM images, a few thinner fibrils with a diameter of around 3.9 nm can be observed (see Figure S25 in the Supporting Information). This value is not too different from the length of a gelator monomer. As proposed for gelator **7** previously,^[9b] these values indicate that the predominant fibers are bundles of either two or four fibrils that form coils. Based on these results we suggest a hierarchical self-assembly process for gel formation (Scheme 2): Initial nucleation of (*R*)-**1** or (*S*)-**1**



Scheme 2. a) Structure of the gelator monomer optimized at the AM1 level of theory as implemented in the CaChe 5.0 program package.^[20] b) Schematic illustration of the hierarchical self-assembly of the gel. Nucleation of the monomer into small oligomers is followed by the formation of fibrils that coil around each other to form fibers. The final step is the formation of entangled networks that entrap the solvent to form the gel.

into hydrogen-bonded dimers and small oligomers is followed by a quick growth into long helical fibrils.^[21] The fibrils can further coil around each other giving rise to helical fibers that are about twice as thick. However, it remains unclear from the AFM and SANS data how many fibrils coil around each other to form a fiber. Fibrils and bundles finally entangle to form a gel and immobilize solvent molecules inside its cavities.

Responsiveness to chemical stimuli: The gel is sensitive to the addition of three different chemical stimuli (Figure 2a). The addition of 1 equiv KPF_6 induces a gel–sol transition, which can be reversed to the gel state by the addition of [2.2.2]cryptand as K^+ scavenger (Figure 2b, top row). This gel–sol phase transition cycle can be followed by ^1H NMR spectroscopy (see Figure S28 in the Supporting Information). As the monomer is CD-silent at wavelengths of 220 and 272 nm, CD spectroscopy can also be used to monitor the gel–sol transition (Figure 2c). The CD signals of the helices are increasingly reduced with increasing K^+ concentration. In a control experiment, NEt_4PF_6 did not induce a gel–sol transition, which shows the weakly coordinating PF_6^- anion does not interfere with the gel structure (see Fig-

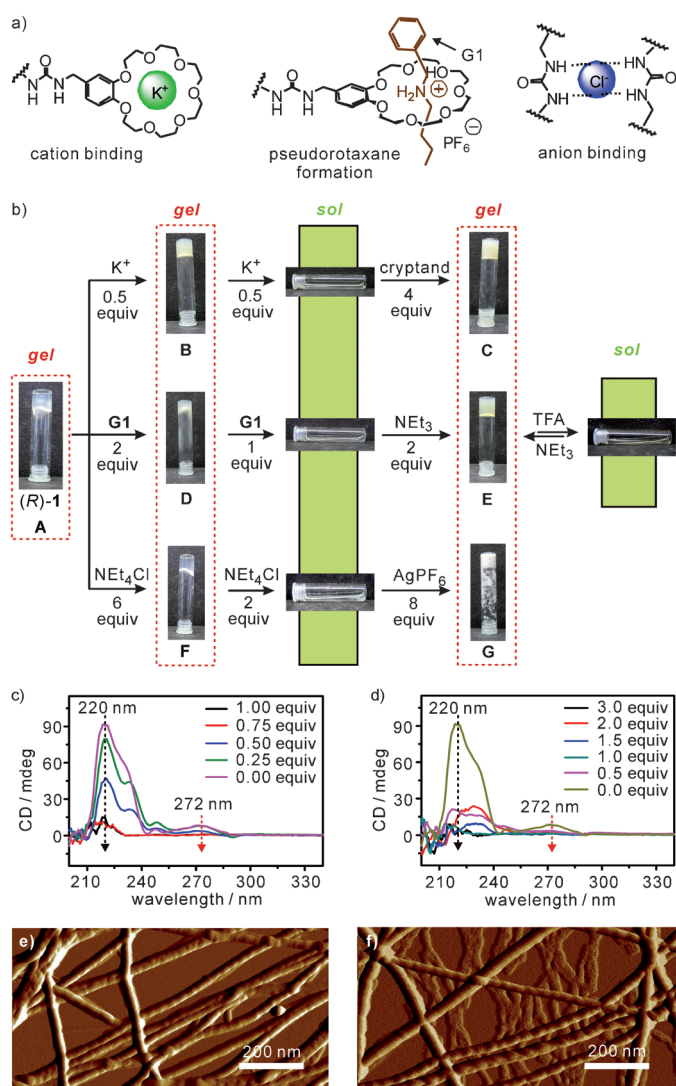


Figure 2. a) Three different chemical stimuli that induce gel–sol transitions: K^+ binding, pseudorotaxane formation, and anion binding. The effects of all three stimuli can be reversed by scavenging the K^+ with a cryptand, deprotonation and subsequent deslipping of the ammonium ion axle, and precipitation of the chloride as AgCl , respectively. b) Supramolecular gel (*R*)-**1** (3.6 wt.% in acetonitrile) and its stimuli-responsive behavior. Gel–sol transitions controlled by K^+ /[2.2.2]cryptand addition (top), acid/base-controlled pseudorotaxane formation with **G1** (middle), and addition of AgCl (bottom). The letters identify the gels as used in the rheology section. Gels are indicated by upside-down test-tubes that show the formation of a solid sample. Sols are represented by horizontal test-tubes that show the fluid behavior of the sample. CD spectral changes during the progressive addition of c) K^+ and d) **G1**. AFM amplitude error images of the gel after addition of e) 0.25 equivalents of KPF_6 and f) 0.5 equivalents of **G1** showing the changes in morphology occurring upon guest addition.

ure S36 in the Supporting Information). The gel remains stable upon addition of up to 0.25 equiv KPF_6 , but its morphology changes to fibers with a smaller helical pitch (Figure 2e). Upon addition of 1 equiv K^+ , nearly all the crown ethers are occupied and charge repulsion likely drives the monomers apart so that the fibrous structure is destroyed.

The second chemical signal that induces a gel–sol transition is the addition of benzyl(*n*-butyl)ammonium hexafluoro-

rophosphate (**G1**; Figure 2a). Again, the intensity of the signal reveals the persistence or destruction of the gel (Figure 2b, middle row): The addition of 2 equiv does not destroy the gel, but 3 equiv of **G1** does. Secondary dialkylammonium ions with at least one unbranched alkyl chain are known to slip through the cavity of benzo-21-crown-7 to form pseudorotaxanes. However, dibenzylammonium does not because the phenyl groups are too bulky to penetrate the crown ether.^[15] Thus, in contrast to **G1**, dibenzylammonium hexafluorophosphate is unable to induce the gel–sol transition in a control experiment (see Figure S39 in the Supporting Information.). Thus, pseudorotaxane formation is the reason behind the gel–sol transition mediated by **G1** as the chemical stimulus. This is also supported by the ¹H NMR spectra (see Figures S37 and S38), which exhibit shifts in signals typical of the threading of **G1** into benzo-21-crown-7.^[9b,15,22] However, only some of the crown ethers appear to be occupied by axles, as signals from free ammonium ions are still observed. This may explain why more than 1 equivalent of the ammonium hexafluorophosphate is required to break the gel. Reversible gel–sol and sol–gel transitions are achieved by the addition of triethylamine (NEt₃); the ammonium ion is deprotonated leading to the dissociation of the pseudorotaxanes and thus restoration of the gel. Subsequent addition of trifluoroacetic acid (TFA) regenerates the ammonium ion, which then slips into the cavity of the crown ether thereby causing destruction of the gel again.

Finally, chloride ions interfere with the urea–urea hydrogen bonding interactions (Figure 2b, bottom row).^[16] Again, a substantial amount of chloride ions (8 equiv of NEt₄Cl) are required to induce the gel–sol transition, which indicates a significant stability of the gel. This gel–sol transition can be reversed by the addition of a stoichiometric amount of AgPF₆, which causes the precipitation of the chloride, but the weakly coordinating PF₆[−] counter ion does not interfere with the gel formation. The resulting NEt₄PF₆ side-product has no significant effect on gel formation, but the gel is more opaque due to presence of the AgCl precipitate. Thus, three different chemical stimuli can be used to induce gel–sol transitions and each of them can be reversed by the appropriate reagents. This opens the way to the construction of logic gates in a similar way to that described earlier for the bis-crown analogue **7**.^[9b]

Rheological characterization of original and switched gels:

All the gels investigated generally show rheological features similar to the original (*R*)-**1** gel (Figure 3). Typically, the storage modulus G' is in the range of 2–5 kPa, increasing with frequency as is typically observed for organogels.^[23] Only for gel **G** is a higher value of around 10 kPa observed, whereas gels **B** and **F** are significantly weaker, with values of about 200–500 Pa. The high frequency limit of the storage modulus, the shear modulus G_0 , can then be related to the number density 1N of elastic connecting points of the gel through Equation (1). From this expression, we can deduce for a G_0 of 5 kPa that the network units have a size of typi-

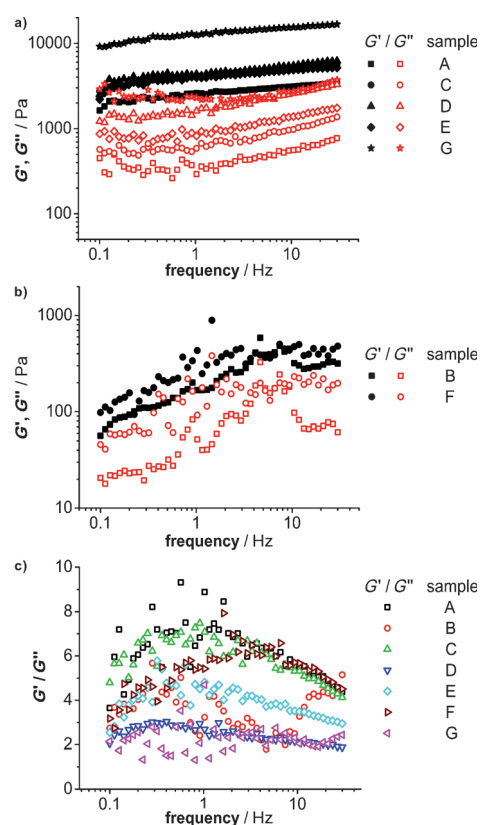


Figure 3. a,b) Storage modulus G' and loss modulus G'' for various gel samples (gelator concentration 41.6 mM in acetonitrile) as a function of oscillatory frequency at 25 °C. c) G'/G'' ratio for the different gel samples as a function of frequency. The letters identify the gels as defined in Figure 2.

cally 9.5 nm. This is much smaller (by about a factor of 10) than the overlap distance deduced from SANS, which means that for such an overlapping network of fibers, a much higher energy than kT is stored per structural unit, which can be explained by the high energy required to deform and bend the rather thick fibers.

$$G_0 = ^1NkT \quad (1)$$

The loss modulus G'' that accounts for the viscous properties of the gel is always substantially smaller, but in general changes in parallel with G' as a function of frequency. Therefore the relative elasticity, as quantified by the ratio G'/G'' , is fairly constant as a function of frequency. The original (*R*)-**1** gel has the highest value (ca. 7 at 1 Hz), and is thus the most elastic gel, the values for the other gels generally ranging from 2 to 7 (Figure 3c). This means that all the gels investigated also have a substantial viscous component, as is typically observed in such self-assembled gels.

Enzyme immobilization in Pickering emulsions: To show the utility of the gelator under study, we provide here a proof-of-principle for the immobilization of an enzyme^[24] in Pickering emulsions (Figure 4a). The aim was to devise a reliable way to deal with phase incompatibility when enzymes

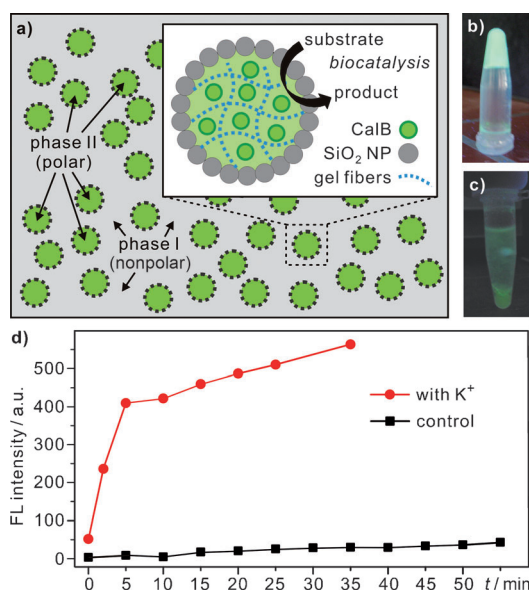


Figure 4. a) Schematic illustration of a Pickering emulsion as used for enzymatic catalysis of organic reactions in organic media. The inner polar phase II contains the enzyme trapped in jellified microparticles that are stabilized by SiO₂ nanoparticles. b) Gel of (*R*)-**1** loaded with FITC-CalB. c) Enzyme release upon addition of KPF₆ to the gel. d) Enzyme release with time from a gel after addition of KPF₆ (red circles) and in a control without added KPF₆ (black squares).

are used for organic reactions that proceed in quite nonpolar organic media. The principle is shown in Figure 4a. The enzyme is trapped within jellified microparticles formed of a polar phase (here acetonitrile/water, 9:1, v/v), which are stabilized by surrounding silica nanoparticles. The microparticles are then immersed in an nonpolar organic phase (here hexane), which contains the reactants for the enzyme-catalyzed reactions. As a result of the large surface area between the two phases, efficient enzyme catalysis is expected to occur within the polar phase inside the particles. Furthermore, the stimuli-responsiveness of the gelator should render the gel itself as well as the carrier systems of the Pickering emulsions capable of controlled enzyme release. For the proof-of-principle experiment described here, lipase B from *Candida antarctica* labeled with fluorescein isothiocyanate (FITC-CalB) was used. The test reaction is the condensation of 1-octanol and octanoic acid to yield the corresponding ester.

Before investigating the Pickering emulsions, enzyme immobilization and release was tested simply in a gel of (*R*)-**1** prepared in the presence of FITC-CalB in acetonitrile/water (9:1) by sonication (Figure 4b). The addition of water to the gel followed by vortexing the sample for 2 min did not result in a significant release of the entrapped FITC-CalB because the layer of water remained fluorescent-silent. The gel decomposed and released the enzyme upon addition of KPF₆, as indicated by the clearly visible green fluorescence distributed in the water phase above the gel (Figure 4c). To follow the enzyme release quantitatively (Figure 4d), the change in concentration of FITC-CalB in the water phase on top of the gel after addition of KPF₆ was followed over

time by measuring the change in fluorescence intensity at $\lambda = 518$ nm (excitation wavelength: 495 nm). Comparison with a control, to which no KPF₆ was added, clearly showed a rapid release of the enzyme in the first few minutes, whereas almost no change was observed in the control. Thus, enzyme release can be efficiently induced by the addition of potassium ions.

Following these experiments that showed the gel of (*R*)-**1** to be capable of immobilizing FITC-CalB and releasing it by means of chemical stimulus, the gelator was used for the preparation of Pickering emulsions. Silica-nanoparticle-stabilized, FITC-CalB-loaded acetonitrile/water (9:1) droplets were jellified in hexane with (*R*)-**1** as described below. Confocal laser scanning microscopy (CLSM) fluorescence imaging (Figure 5a) demonstrated the successful formation of the emulsion. Green fluorescent microparticles were formed with diameters in the range of 5–10 μm , with no fluorescence being observed from the surrounding hexane phase. The enzyme is thus exclusively located in the polar-phase microparticles. Figure 5a clearly shows that the enzyme is distributed nonhomogeneously within the microparticles, which can be attributed to physical adsorption on the gel network.^[25] Centrifugation (6000 rpm, 10 min) produced a fluorescent sediment with a nonfluorescent hexane phase, which proves that the droplets can be removed from the organic phase very easily (Figure 5b). As the droplets are stable and do not lose their integrity during centrifugation, they can be reused a multiple number of times. Figure 5c,d shows the situation after the addition of K⁺ to the Pickering emulsion. Clearly the droplets release FITC-CalB when the gel inside turns into a sol and the trapped enzyme can be regained after gentle centrifugation (6000 rpm, 30 s). K⁺-induced enzyme release has again been followed over time and compared with a control experiment in which no potassium ions were added. As noted above for the gel, the increase in fluorescence intensity in the supernatant solution, and with it the enzyme release, is much faster when the gel is destroyed by the addition of K⁺ (Figure 5e).

The CD spectra of the native enzyme and that released and recollected from the microparticles (Figure 5f) are very similar and exhibit the typical double absorbance at 208 and 220 nm indicative of α -helices that are a prominent structural feature in CalB. The similarity of both CD spectra indicates no or only very minor structural differences between the native enzyme and that released from the emulsion microparticles. Consequently, K⁺ can also be used as a trigger to release the immobilized enzymes from the droplets in Pickering emulsions in which the enzyme is likely trapped in its native conformation. To the best of our knowledge, this represents the first example of the use of supramolecular gels in Pickering emulsions for controlled enzyme immobilization and release.

The activity of the immobilized enzyme was studied in the esterification of 1-octanol and 1-octanoic acid as a model reaction (Figure 5g,h). The specific activity of the lipase immobilized in the gelled Pickering emulsion microparticles (65.70 U mg⁻¹) is almost 20 times greater than that of the

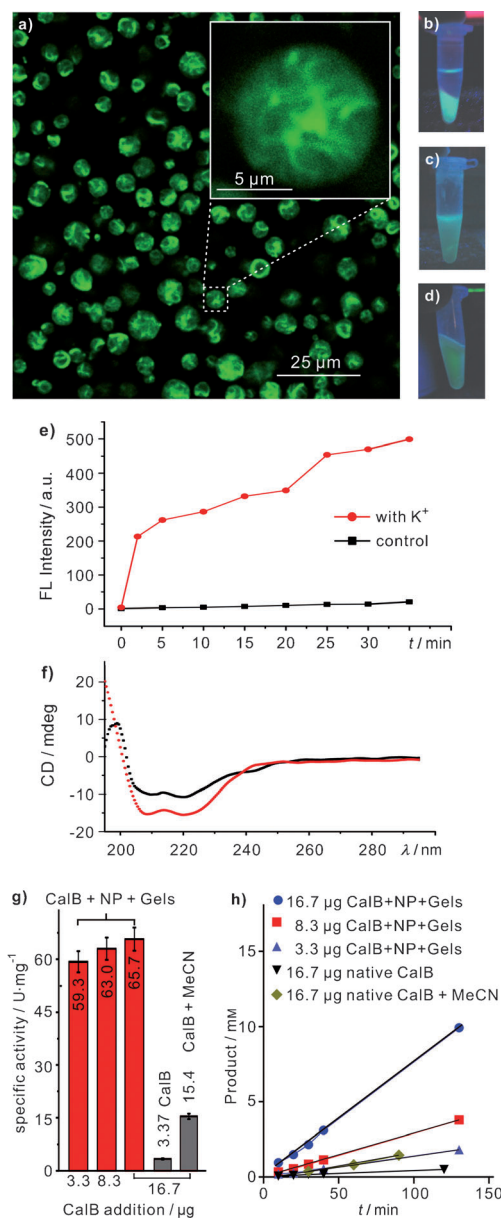


Figure 5. a) Fluorescence microscopy image of jellified acetonitrile/water (9:1) microparticles loaded with FITC-CalB and stabilized by 140 nm SiO₂ nanoparticles (nonpolar phase I: hexane; polar phase II: water/acetonitrile, 9:1; conc. of (R)-1 in phase II: 1.8 wt.%; conc. of SiO₂-NP: 1.0 wt. %). Inset: Enlarged CLSM image of a jellified FITC-CalB microparticle. b) Jellified Pickering emulsion droplets loaded with FITC-CalB as a fluorescent sediment in hexane after centrifugation. c) Release of FITC-CalB from the microparticles induced by decantation of the hexane phase and KPF₆ addition. d) Released enzyme in the supernatant above the microparticles after centrifugation at 6000 rpm for 10 min and addition of 15 mg KPF₆ in water (red circles) or water alone (black squares). e) Changes in fluorescence intensity in the supernatant after centrifugation. f) CD spectra of native CalB (red line) and CalB released from jellified Pickering emulsion droplets (black line). g) Specific activities of CalB (grey) in biphasic hexane/water systems with or without acetonitrile as control (amounts identical to the amounts used in the experiment with Pickering emulsions) and CalB immobilized in Pickering emulsions (red line). h) Linear dependence of the initial conversion of substrates with time at different concentrations of enzymes in the emulsion microparticles.

same amount of native enzyme in a liquid water/hexane biphasic system (3.37 U mg⁻¹) containing the same overall amount of water as that used to prepare the Pickering emulsions. To include a control that contains exactly the same amounts of all the solvents used in the experiments with the Pickering emulsions, this experiment was repeated in a biphasic system containing hexane, water, and acetonitrile. In this case the specific activity is somewhat higher than in the water/hexane system, but still lower by a factor of four than that obtained in the Pickering emulsions. This increased specific activity can be attributed to the considerably larger interfacial area of the SiO₂-nanoparticle-stabilized microparticles, which improves the mass transfer between the two phases and the accessibility to the enzyme catalyst.^[12,26] Interestingly, different amounts of lipase in the gel particles yield almost the same specific activity (Figure 5g). Also, the initial reaction rates of the esterification reaction increase with enzyme concentration. This reflects the open network structure of the gel and the low resistance to the diffusion of the rather small substrate molecules within the particles compared with the much larger enzyme molecules, which are efficiently trapped. These experiments show the utility of gelator (R)-1 in enzyme-catalyzed reactions in organic media.

Conclusion

A low-molecular-weight bis-urea gelator has been prepared, the chirality of which determines the helicity of the fibers formed during gelation. It is versatile and forms gels in a number of different solvents with quite low critical gelation concentrations. In acetonitrile, it can even be regarded as a supergelator as the CGC is less than 0.1 wt.%. The gelator is substituted with a crown ether making it susceptible to different chemical stimuli that induce gel-sol transitions: K⁺ ion binding, pseudorotaxane formation between dialkylammonium ions and the crown ether, and interference of the urea-urea hydrogen bonds through the interactions with chloride anions. Each of these stimuli can be reversed such that the gel-sol transitions are reversible. Enzymes such as lipase B from *Candida antarctica* can be immobilized within the gel and released on demand by the addition of a chemical stimulus, as exemplarily shown with K⁺. The gelator is the first low-molecular-weight gelator used for enzyme immobilization in Pickering emulsions. It thus contributes to solving the phase problem that often exists when enzymes are to be used to catalyze organic reactions in nonpolar organic media. The catalytic activity of CalB in Pickering emulsions is significantly higher than that in the corresponding biphasic solvent system. As the microparticles are stable enough to withstand centrifugation, the catalyst can easily be separated from the reaction mixture.

Experimental Section

Gelation experiments and stimuli responsiveness of the gels: The gelator and the solvent were placed in a capped test-tube, sonicated for 3 min, and if necessary heated until the solid dissolved. The sample vial was cooled to 25 °C and left to stand for 1 h under ambient conditions. The state was evaluated by the “stable to inversion of a test-tube” method. Gel–sol transition temperatures T_{gs} were determined by the “dropping-ball method”.^[27] A small ball (166 mg) was placed on top of the gel in a test-tube (internal diameter 1.0 cm), which was slowly heated in a water bath at a rate of 1 K min⁻¹. T_{gs} is defined as the temperature at which the ball reaches the bottom of the test-tube. Dropping-ball experiments were carried out at least in duplicate, and the T_{gs} values obtained were reproducible to within ±1 °C. To examine the guest-induced stimuli responsive behavior, the guest compound was added to the test-tube containing the already-prepared gel. Subsequently, the capped test-tube was sonicated for 5 min. The sample vial was left to stand for 15 min under ambient conditions. The state was evaluated as described above.

Study of enzyme immobilization and release from the supramolecular gel: The gel loaded with FITC-CalB was prepared by dissolving FITC-CalB (25 µL, 0.335 mg mL⁻¹ of the enzyme) and the gelator (3.15 mg) in acetonitrile (250 µL) followed by sonication and gel formation as described above. Then, in two experiments, either deionized water (750 µL) or a solution of KPF₆ (10 mg) in deionized water (750 µL) was added to the gel sample. For both samples, the amount of released FITC-CalB was followed by monitoring the change in fluorescence intensity (excitation wavelength: 495 nm) at 518 nm, which corresponds to the fluorescence maximum of FITC-CalB.

Immobilization and release of enzymes in/from Pickering emulsions: For the immobilization of CalB in Pickering emulsions, the gelator (6.3 mg) and an aqueous solution of CalB (50 µL, 0.335 mg mL⁻¹ of the enzyme) were added to acetonitrile (450 µL). The enzyme/gelator mixture (500 µL) was homogenized in dispersions of SiO₂@TMODS nanoparticles (silica nanoparticles 140 nm in diameter that are made hydrophobic with trimethoxy(octadecyl)silane (TMODS)) in hexane (1.5 mL) at room temperature. Jellified Pickering emulsions entrapping the enzyme were characterized by confocal laser scanning microscopy (CLSM, Leica DM IRBE confocal laser scanning microscope at an excitation wavelength of 488 nm). The CalB enzyme content was determined according to a Bradford assay.^[28] To examine the enzyme release from the Pickering emulsions, the same procedure was carried out as described for the enzyme release studies from the gel, except that the samples were centrifuged at 6000 rpm for 10 min to remove the hexane layer before the addition of deionized water or KPF₆ solution (750 µL), respectively.

Assessment of the catalytic performance of free and immobilized CalB: CalB activity was determined by using the esterification of 1-octanol and octanoic acid as the test reaction. Typically, the Pickering emulsion in hexane (2 mL) containing different amounts of CalB were introduced into hexane (13 mL) containing a calculated amount of substrate. For the control experiment, CalB (50 µL) with or without acetonitrile (450 µL) was introduced into a solution of the substrate in hexane (14.5 mL). The overall water content was the same in all experiments. The esterification reactions were all carried out under the same conditions with 100 mM 1-octanol and 100 mM octanoic acid in hexane on a rotating shaker at 80 rpm at room temperature for 130 min. After 10, 20, 30, 40, and 130 min, aliquots (100 µL) were removed from the mixture and centrifuged at 14500 rpm for 20 s. Subsequently the supernatants were analyzed for ester concentration by gas chromatography (Shimadzu 2010; BPX5 column from SGE: length 25 m, ID 0.22 mm; film thickness: 0.25 µm; detector: FID at 300 °C; injector: 275 °C, injection volume: 1 µL, split model; temperature program: start temperature 80 °C, hold for 0.5 min, temperature rise 20 °C min⁻¹ from 80 to 170 °C and 5 °C min⁻¹ from 170 °C to the end temperature 200 °C). The concentrations of the octyl octanoate product were calculated from the area of the chromatographic peak at a retention time of 10.01 min. The catalytic activity was assessed in terms of octyl octanoate units. One unit (U) correlates to the production of one µmol octyl octanoate per minute. The specific activity is expressed as units per milligram of protein (U mg⁻¹).

Acknowledgements

We thank the Deutsche Forschungsgemeinschaft for financial support (SCHA 893/5 and SFB 765). Z.Q. is grateful to the China Scholarship Council (CSC) for a Ph. D. fellowship. We thank Leonardo Chiappisi for performing the SANS measurements. We acknowledge Marie-Sousai Appavou (JCNS) for help with the SANS experiments and the JCNS for granting beamtime.

- [1] D. A. Fletcher, R. D. Mullins, *Nature* **2010**, *463*, 485–492.
- [2] S.-i. Tamaru, M. Ikeda, Y. Shimidzu, S. Matsumoto, S. Takeuchi, I. Hamachi, *Nat. Commun.* **2010**, *1*, 20.
- [3] For selected recent reviews, see: a) N. M. Sangeetha, U. Maitra, *Chem. Soc. Rev.* **2005**, *34*, 821–836; b) R. G. Weiss, *Acc. Chem. Res.* **2006**, *39*, 489–497; c) P. Dastidar, *Chem. Soc. Rev.* **2008**, *37*, 2699–2715; d) L. E. Buerkle, S. J. Rowan, *Chem. Soc. Rev.* **2012**, *41*, 6089–6102; e) A. Noro, M. Hayashi, Y. Matsushita, *Soft Matter* **2012**, *8*, 2416–2429; f) D. K. Smith in *Supramolecular Chemistry: From Molecules to Nanomaterials* (Eds.: P. A. Gale, J. W. Steed), Wiley, Hoboken, **2012**, pp. 3355–3376; g) H. Svobodová, V. Noponen, E. Kolehmainen, E. Sievanen, *RSC Adv.* **2012**, *2*, 4985–5007; h) S. Seiffert, J. Sprakel, *Chem. Soc. Rev.* **2012**, *41*, 909–930; i) D. Das, T. Kar, P. K. Das, *Soft Matter* **2012**, *8*, 2348–2365; j) E. A. Appel, J. del Barrio, X. J. Loh, O. A. Scherman, *Chem. Soc. Rev.* **2012**, *41*, 6195–6214.
- [4] For examples of gels responsive to different stimuli, see: a) T. Ogoshi, Y. Takashima, H. Yamaguchi, A. Harada, *J. Am. Chem. Soc.* **2007**, *129*, 4878–4879; b) H. Maeda, *Chem. Eur. J.* **2008**, *14*, 11274–11282; c) G. O. Lloyd, J. W. Steed, *Nat. Chem.* **2009**, *1*, 437–442; d) J. H. Kim, M. Seo, Y. J. Kim, S. Y. Kim, *Langmuir* **2009**, *25*, 1761–1766; e) T. Tazawa, S. Yagai, Y. Kikkawa, T. Karatsu, A. Kitamura, A. Ajayaghosh, *Chem. Commun.* **2010**, *46*, 1076–1078; f) J. A. Foster, J. W. Steed, *Angew. Chem.* **2010**, *122*, 6868–6874; *Angew. Chem. Int. Ed.* **2010**, *49*, 6718–6724; g) Y. Suzaki, T. Taira, K. Osakada, *J. Mater. Chem.* **2011**, *21*, 930–938; h) D. Díaz Díaz, D. Kühbeck, R. J. Koopmans, *Chem. Soc. Rev.* **2011**, *40*, 427–448; i) Y.-S. Su, J.-W. Liu, Y. Jiang, C.-F. Chen, *Chem. Eur. J.* **2011**, *17*, 2435–2441; j) X. Wang, L. Zhou, H. Wang, Q. Luo, J. Xu, J. Liu, *J. Colloid Interface Sci.* **2011**, *353*, 412–419; k) F. Rodríguez-Llansola, J. F. Miravet, B. Escuder, *Chem. Commun.* **2011**, *47*, 4706–4708; l) V. Lozano, R. Hernandez, A. Arda, J. Jimenez-Barbero, C. Mijangos, M.-J. Perez-Perez, *J. Mater. Chem.* **2011**, *21*, 8862–8870; m) L. Chen, Y.-K. Tian, Y. Ding, Y.-J. Tian, F. Wang, *Macromolecules* **2012**, *45*, 8412–8419; n) L. Tan, Y. Liu, W. Ha, L.-S. Ding, S.-L. Peng, S. Zhang, B.-J. Li, *Soft Matter* **2012**, *8*, 5746–5749.
- [5] For selected examples, see: a) X. Liao, X. Chen, G. Chen, X. Liu, W. Chen, F. Chen, M. Jiang, *Angew. Chem.* **2010**, *122*, 4511–4515; *Angew. Chem. Int. Ed.* **2010**, *49*, 4409–4413; b) A. Harada, R. Kobayashi, Y. Takashima, A. Hashidzume, H. Yamaguchi, *Nat. Chem.* **2011**, *3*, 34–37; c) S. Tamesue, Y. Takashima, H. Yamaguchi, S. Shinkai, A. Harada, *Angew. Chem.* **2010**, *122*, 7623–7626; *Angew. Chem. Int. Ed.* **2010**, *49*, 7461–7464; d) S. Dong, Y. Luo, X. Yan, B. Zheng, X. Ding, Y. Yu, Z. Ma, Q. Zhao, F. Huang, *Angew. Chem.* **2011**, *123*, 1945–1949; *Angew. Chem. Int. Ed.* **2011**, *50*, 1905–1909; e) T. Akutagawa, K. Kakiuchi, T. Hasegawa, S. Noro, T. Nakamura, H. Hasegawa, S. Mashiko, J. Becher, *Angew. Chem.* **2005**, *117*, 7449–7453; *Angew. Chem. Int. Ed.* **2005**, *44*, 7283–7287; f) A. A. Sobczuk, S. Tamaru, S. Shinkai, *Chem. Commun.* **2011**, *47*, 3093–3095; g) I. Hwang, W. S. Jeon, H. J. Kim, D. Kim, H. Kim, N. Selvapalam, N. Fujita, S. Shinkai, K. Kim, *Angew. Chem.* **2007**, *119*, 214–217; *Angew. Chem. Int. Ed.* **2007**, *46*, 210–213; h) T. Becker, C. Y. Goh, F. Jones, M. J. McIlldowie, M. Mocerino, M. I. Ogdan, *Chem. Commun.* **2008**, 3900–3902; i) X. Cai, K. Liu, J. Yan, H. Zhang, X. Hou, Z. Liu, Y. Fang, *Soft Matter* **2012**, *8*, 3756–3761; j) J. Liu, P. He, J. Yan, X. Fang, J. Peng, K. Liu, Y. Fang, *Adv. Mater.* **2008**, *20*, 2508–2511; k) X. Yan, D. Xu, X. Chi, J. Chen, S. Dong, X. Ding, Y. Yu, F. Huang, *Adv. Mater.* **2012**, *24*, 362–369.

- [6] a) J. H. Jung, H. Kobayashi, M. Masuda, T. Shimizu, S. Shinkai, *J. Am. Chem. Soc.* **2001**, *123*, 8785–8789; b) H. Engelkamp, S. Middelbeek, R. J. M. Nolte, *Science* **1999**, *284*, 785–788.
- [7] a) G. M. Whitesides, B. Grzybowski, *Science* **2002**, *295*, 2418–2421; b) X. Yang, G. Zhang, D. Zhang, *J. Mater. Chem.* **2011**, *21*, 38–50; c) Z.-X. Liu, Y. Feng, Z.-C. Yan, Y.-M. He, C.-Y. Liu, Q.-H. Fan, *Chem. Mater.* **2012**, *24*, 3751–3757; d) M. D. Segarra-Maset, V. J. Nebot, J. F. Miravet, B. Escuder, *Chem. Soc. Rev.* **2013**, DOI: 10.1039/C2CS35436E.
- [8] A. R. Hirst, B. Escuder, J. F. Miravet, D. K. Smith, *Angew. Chem.* **2008**, *120*, 8122–8139; *Angew. Chem. Int. Ed.* **2008**, *47*, 8002–8018.
- [9] a) H. Komatsu, S. Matsumoto, S.-i. Tamaru, K. Kaneko, M. Ikeda, I. Hamachi, *J. Am. Chem. Soc.* **2009**, *131*, 5580–5585; b) Z. Qi, P. Malo de Molina, W. Jiang, Q. Wang, K. Nowosinski, A. Schulz, M. Gradzielski, C. A. Schalley, *Chem. Sci.* **2012**, *3*, 2073–2082.
- [10] a) Y. Gao, F. Zhao, Q. Wang, Y. Zhang, B. Xu, *Chem. Soc. Rev.* **2010**, *39*, 3425–3433; b) A. E. David, A. J. Yang, N. S. Wang, *Methods Mol. Biol.* **2011**, *679*, 49–66.
- [11] S. U. Pickering, *J. Chem. Soc.* **1907**, *91*, 2001–2021.
- [12] a) C. Wu, S. Bai, M. B. Ansorge-Schumacher, D. Wang, *Adv. Mater.* **2011**, *23*, 5694–5699; b) Z. Wang, M. C. M. van Oers, F. P. J. T. Rutjes, J. C. M. van Hest, *Angew. Chem.* **2012**, *124*, 10904–10908; *Angew. Chem. Int. Ed.* **2012**, *51*, 10746–10750.
- [13] a) J. H. van Esch, S. De Feyter, R. M. Kellogg, F. De Schryver, B. L. Feringa, *Chem. Eur. J.* **1997**, *3*, 1238–1243; b) J. H. van Esch, F. Schoonbeek, M. de Loos, H. Kooijman, A. L. Spek, R. M. Kellogg, B. L. Feringa, *Chem. Eur. J.* **1999**, *5*, 937–950; c) F. S. Schoonbeek, J. H. van Esch, R. Hulst, R. M. Kellogg, B. L. Feringa, *Chem. Eur. J.* **2000**, *6*, 2633–2643; d) A. Arnaud, L. Bouteiller, *Langmuir* **2004**, *20*, 6858–6863; e) Y. Jeong, K. Hanabusa, H. Masunaga, I. Akiba, K. Miyoshi, S. Sakurai, K. Sakurai, *Langmuir* **2005**, *21*, 586–594; f) L. Bouteiller, O. Colombani, F. Lortie, P. Terech, *J. Am. Chem. Soc.* **2005**, *127*, 8893–8898; g) C. Wang, D. Zhang, D. Zhu, *Langmuir* **2007**, *23*, 1478–1482; h) M. Bellot, L. Bouteiller, *Langmuir* **2008**, *24*, 14176–14182.
- [14] a) G. W. Gokel, W. M. Leevy, M. E. Weber, *Chem. Rev.* **2004**, *104*, 2723–2750; b) F. Huang, H. W. Gibson, *Prog. Polym. Sci.* **2005**, *30*, 982–1018; c) W. Jiang, C. A. Schalley, *Beilstein J. Org. Chem.* **2010**, *6*, 14.
- [15] For examples of pseudo-rotaxanes formed with benzo-21-crown-7, see: a) C. Zhang, S. Li, J. Zhang, K. Zhu, N. Li, F. Huang, *Org. Lett.* **2007**, *9*, 5553–5556; b) C. Zhang, K. Zhu, S. Li, J. Zhang, F. Wang, M. Liu, N. Li, F. Huang, *Tetrahedron Lett.* **2008**, *49*, 6917–6920; c) W. Jiang, A. Schäfer, P. C. Mohr, C. A. Schalley, *J. Am. Chem. Soc.* **2010**, *132*, 2309–2320; d) X. Yan, M. Zhou, J. Chen, X. Chi, S. Dong, M. Zhang, X. Ding, Y. Yu, S. Shao, F. Huang, *Chem. Commun.* **2011**, *47*, 7086–7088; e) W. Jiang, D. Sattler, K. Rissanen, C. A. Schalley, *Org. Lett.* **2011**, *13*, 4502–4505.
- [16] J. W. Steed, *Chem. Soc. Rev.* **2010**, *39*, 3686–3699.
- [17] R. M. Versteegen, R. P. Sijbesma, E. W. Meijer, *Macromolecules* **2005**, *38*, 3176–3184.
- [18] M.-O. M. Piepenbrock, G. O. Lloyd, N. Clarke, J. W. Steed, *Chem. Commun.* **2008**, 2644–2646.
- [19] A. Lohr, M. Lysetska, F. Würthner, *Angew. Chem.* **2005**, *117*, 5199–5202; *Angew. Chem. Int. Ed.* **2005**, *44*, 5071–5074.
- [20] Calculations were performed with the CaChe 5.0 program package, Fujitsu, Krakow/Poland.
- [21] P. Jonkheijm, P. van der Schoot, A. P. H. J. Schenning, E. W. Meijer, *Science* **2006**, *313*, 80–83.
- [22] a) W. Jiang, H. D. F. Winkler, C. A. Schalley, *J. Am. Chem. Soc.* **2008**, *130*, 13852–13853; b) W. Jiang, C. A. Schalley, *Proc. Natl. Acad. Sci. USA* **2009**, *106*, 10425–10429.
- [23] a) P. Terech, S. Friol, *Tetrahedron* **2007**, *63*, 7366–7374; b) P. Lo Nostro, R. Ramsch, E. Fratini, M. Lagi, F. Ridi, E. Carretti, M. Ambrosi, B. W. Ninham, P. Baglioni, *J. Phys. Chem. B* **2007**, *111*, 11714–11721; c) M. Burkhardt, S. Kinzel, M. Gradzielski, *J. Colloid Interface Sci.* **2009**, *331*, 514–521.
- [24] For a few selected examples, see: a) K. Martinek, A. Levashov, Y. Khmel'nitsky, N. Klyachko, I. Berezin, *Science* **1982**, *218*, 889–891; b) C. Pizarro, M. A. Fernández-Torroba, C. Benito, J. M. González-Sáiz, *Biotechnol. Bioeng.* **1997**, *53*, 497–506; c) Q. Wang, Z. Yang, Y. Gao, W. Ge, L. Wang, B. Xu, *Soft Matter* **2008**, *4*, 550–553.
- [25] a) M. B. Ansorge-Schumacher, *Immobilization of biological catalysts*, Wiley-VCH, Weinheim, **2008**; b) L. Cao, *Carrier-bound Immobilized Enzymes: Principles, Applications and Design*, Wiley-VCH, Weinheim, **2005**; c) A. M. Klibanov, *Science* **1983**, *219*, 722–727; d) W. Tischer, F. Wedekind, *Top. Curr. Chem.* **1999**, *200*, 95–126.
- [26] a) M. B. Ansorge-Schumacher, *Mini-Rev. Org. Chem.* **2007**, *4*, 243–245; b) G. Carrea, S. Riva, *Angew. Chem.* **2000**, *112*, 2312–2341; *Angew. Chem. Int. Ed.* **2000**, *39*, 2226–2254; c) C. Wu, M. Kraume, M. B. Ansorge-Schumacher, *ChemCatChem* **2011**, *3*, 1314–1319; d) D. J. Cole-Hamilton, *Science* **2010**, *327*, 41–42.
- [27] P. Terech, C. Rossat, F. Volino, *J. Colloid Interface Sci.* **2000**, *227*, 363–370.
- [28] M. M. Bradford, *Anal. Biochem.* **1976**, *72*, 248–254.

Received: January 18, 2013

Revised: May 10, 2013

Published online: July 10, 2013